Available online at www.sciencedirect.com

SCIENCE DIRECT®

Lithos 87 (2006) 174–192

LITHOS

www.elsevier.com/locate/lithos

The isotopic composition of zircon and garnet: A record of the metamorphic history of Naxos, Greece

L. Martin [a,*], S. Duchêne [a], E. Deloule [a], O. Vanderhaeghe [b]

[a] *CRPG, UPR-CNRS 2300, BP 20, 54501 Vandœuvre, France*
[b] *G2R, UMR-CNRS 7566, BP 239, 54506 Vandœuvre, France*

Received 13 November 2003; accepted 2 June 2005
Available online 6 October 2005

Abstract

Growth of zircon with respect to that of garnet has been studied using a combination of petrography, U–Pb dating and oxygen isotope analysis. The aim is to document the mechanism and pressure–temperature conditions of zircon growth during metamorphism in order to better constrain the Tertiary metamorphic history of Naxos, Greece. Two metamorphisms are recognised: (1) an Eocene Franciscan metamorphism (M1) and (2) a widespread Miocene Barrovian metamorphism (M2) that increases from greenschist facies up to partial melting. An amphibolite sample contains zircon crystals characterised by a magmatic core and two metamorphic rims, denoted as A and B, dated at 200–270, 42–69, and 14–19 Ma, respectively. The first metamorphic rim A ($\delta^{18}O=7\pm1‰$) preserves the $\delta^{18}O$ value of the magmatic core ($6.2\pm0.8‰$), whereas rim B is characterised by higher $\delta^{18}O$ values ($7.8\pm1.8‰$). These observations indicate the formation of A rims by solid-state recrystallisation in a closed system with regard to oxygen and those of B in an open system. Compositional zoning in garnet is interpreted as the result of decompressional heating. Zircon B rims and garnet rims display similar $\delta^{18}O$ values which indicates a contemporaneous growth of garnet and zircon rims during the Miocene Barrovian event (M2). Calcic gneiss and metapelite samples contain zircon crystals with single metamorphic overgrowths aged 41–57 Ma. $\delta^{18}O$ values measured in zircon overgrowths ($11.8\pm1.4‰$) from the calcic gneiss are similar to those measured in garnet rims ($11.4\pm1.1‰$) from the same rock. This suggests that garnet rims and zircon overgrowths grew during the high pressure–low temperature event in equilibrium with prograde fluids. In the metapelite sample, $\delta^{18}O$ values are similar in garnet cores ($14.8\pm0.2‰$) and in zircon metamorphic overgrowths ($14.2\pm0.5‰$). As zircon overgrowths have been dated at ca. 50 Ma by U–Pb, garnet cores and zircon overgrowths are interpreted to have grown during the high pressure event.

As demonstrated here for the island of Naxos, correlating the crystallisation of zircon with that of metamorphic index minerals such as garnet using stable isotope composition and U–Pb determination is a powerful tool for deciphering the mechanism of zircon growth and pin-pointing zircon crystallisation within the metamorphic history of a terrain. This approach is potentially hampered by an inability to verify the degree of textural equilibrium of zircon with other mineral phases, and the possible preservation (in metamorphic rims) of isotopic signatures from pre-existing zircon when they form by recrystallisation.

* Corresponding author. Tel.: +33 3 83 59 42 42; fax: +33 3 83 51 17 98.
E-mail address: lmartin@crpg.cnrs-nancy.fr (L. Martin).

0024-4937/$ - see front matter
doi:10.1016/j.lithos.2005.06.016

Nevertheless, this study illustrates the application of this approach in providing key constraints on the timing and mechanism of growth of minerals important to understanding metamorphic petrogenesis.

Keywords: U/Pb; Absolute age; O-18/O-16; Garnet; Zircon; Naxos

1. Introduction

Constraint on the timing of a metamorphic event is nowadays often accomplished by U–Pb isotopic dating of zircon. Lee et al. (1997), and Cherniak and Watson (2000) experimentally determined that the closure temperature of the U–Th–Pb isotopic system in zircon is greater than 900 °C and that Pb isotope ratios will not be altered by volume diffusion under most geologic conditions. Consequently, zircon is able to preserve multistage magmatic and metamorphic histories (e.g., Zeck and Whitehouse, 1999; Möller et al., 2002). Metamorphic zircon growth occurs as thin overgrowths or rims around relict cores or as small equant grains (Hoskin and Schaltegger, 2003) from which U–Pb ages can be determined using high mass resolution ion microprobes (Ireland, 1995). However, Rizvanova et al. (2000) showed that the U–Th–Pb system can be disturbed at temperatures lower than 900 °C in the presence of fluids. Additionally, neither the mechanisms of growth nor the stability field of zircon during metamorphism are well constrained. Previous studies have shown that zircon can grow (i) in closed system at the rock scale by solid-state recrystallisation of protolith zircon (Hoskin and Black, 2000), by dissolution–recrystallisation (Pidgeon, 1992; Pan, 1997), or by destabilisation of Zr-bearing accessory (e.g., ilmenite; Bingen et al., 2001) and major minerals (e.g., amphibole and garnet; Fraser et al., 1997), and (ii) in open systems, during partial melting (Roberts and Finger, 1997) or fluid circulation (Williams et al., 1996).

In order to recover pressure–temperature conditions of zircon crystallisation, several attempts have been made to link zircon growth to an index mineral of metamorphism. (1) Net transfer reactions involving the breakdown or crystallisation of a Zr-bearing phase such as hornblende or garnet have been identified (Fraser et al., 1997). (2) Mineral inclusions preserved in zircon can provide direct information of a mineral assemblage before and during zircon growth (Gebauer et al., 1997; Hermann et al., 2001). However, as pointed out by Rubatto (2002) such inclusions are rare. (3) The comparison of trace element patterns in zircon and other minerals such as garnet or feldspar can be used to assess their concurrent growth (Peucat et al., 1995; Schaltegger et al., 1999; Rubatto, 2002). This method has to be used with caution because of the wide range of possible zircon trace element compositions (Hoskin and Ireland, 2000; Rubatto, 2002), the possible existence of an inherited component when solid-state recrystallisation of protolith zircon occurs (Hoskin and Black, 2000), and because the partitioning of trace elements between zircon and other phases is not well quantified. In this respect, the evaluation of trace element partitioning coefficients between garnet and zircon in equilibrium at granulite facies grade (Rubatto, 2002) appears to be a potential tool to link zircon to garnet growth (Whitehouse and Platt, 2003).

Another way to correlate metamorphic zircon rims with garnet growth that has, to our knowledge, not previously been investigated is via oxygen isotope compositions. On the one hand, oxygen isotope provide information on the closure of the system with respect to fluids; and on the other hand, they are good tracers of concomitant growth of garnet and zircon as there is no fractionation of oxygen isotope at equilibrium between them (Zheng, 1993; Valley et al., 1994).

In this study, the oxygen isotope composition of zircon and garnet are measured for a suite of samples from Naxos, Greece, in order to first investigate zircon growth mechanisms and second to discuss the geological significance of zircon U–Pb ages. Naxos lies in the Aegean region, at the north of the Hellenic subduction zone (Fig. 1A). Naxos displays a migmatite dome forms rimmed by a metasedimentary sequence (marble and schist, “Middle unit”, Fig. 1B). Metabasites locally cross-cut the metasedimen-

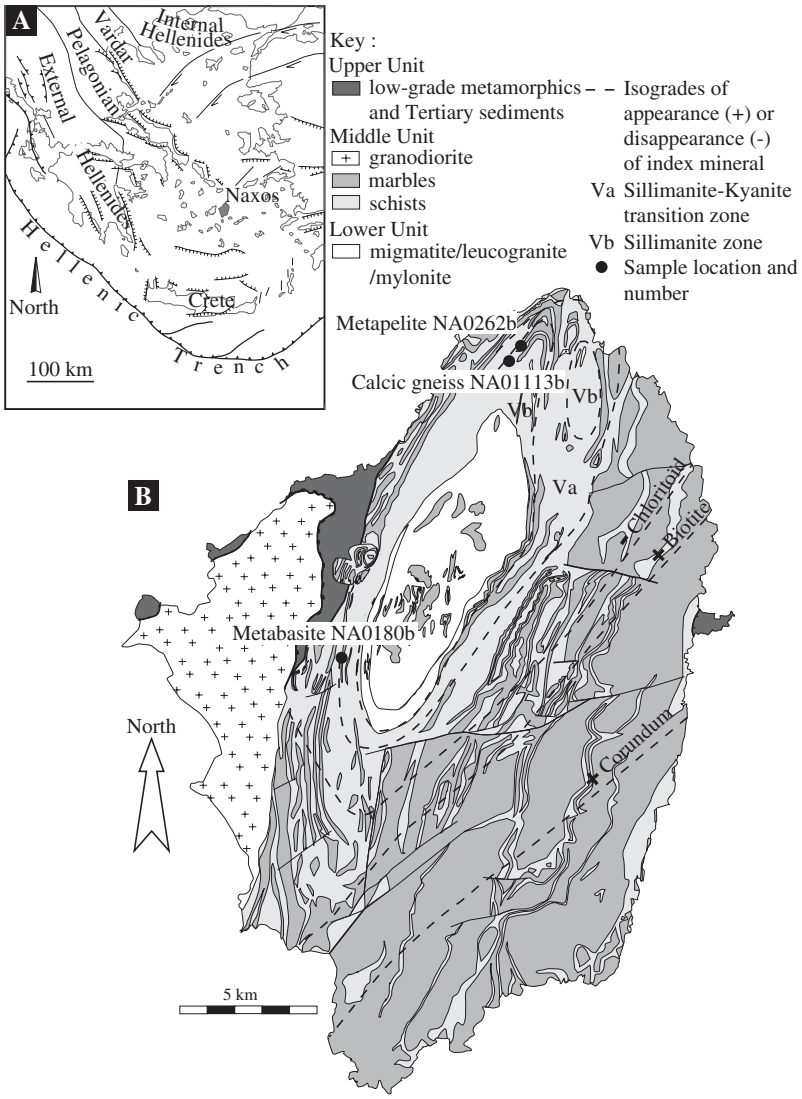

Fig. 1. Geology of Naxos. A: Location of Naxos on a schematic map of the Aegean region. B: Geological map of Naxos by Vanderhaeghe (2004) (after Jansen, 1973). Isograds are modified from Jansen and Schuiling (1976). Sample locations are indicated by black dots.

tary sequence or are interlayered with them. Two metamorphic events are recognised (Jansen and Schuiling, 1976): (1) a Franciscan metamorphism (M1) recorded by rare blueschist relics in the south of the island. Peak pressure–temperature conditions were estimated at 12 kbar, 470 °C (occurrence of jadeite, Avigad, 1998) to 530 °C (Jansen and Schuiling, 1976). This event was dated by Ar–Ar, K–Ar, and Rb–Sr methods on white micas at 45 ± 5 Ma (Andriessen et al., 1979; Wijbrans and McDougall, 1986; Andriessen, 1991) (2) A widespread Barrovian metamorphism (M2) affects the whole metasedimentary sequence, and increases from greenschist facies (T~380 °C) in the south to partial melting in the core (700 °C, Jansen and Schuiling, 1976). On the basis of this thermal evolution, Jansen (1973) and Jansen and Schuiling (1976) distinguished mineral isograds that correspond to isotherms during the M2 event (Fig.

1B). Isograde and the main foliation are concentric with the structure of the dome and the latter is generally marked by M2 metamorphic minerals, such as biotite. Partial melting in the migmatitic core was dated at 16–20 Ma by U–Pb dating on zircon (Keay, 1998; Keay et al., 2001).

U–Pb dating on zircon by Keay (1998) provide evidence for different age components at 28, 42, 54 Ma in the migmatitic core and 35, 42, 48, 64 Ma outside the core. These data suggest that several zircon growth stages occurred during the M1 metamorphism and between M1 and M2. On the basis of petrographic interpretations, the author explained the numerous modelled growth stages by precipitation from successive infiltrating fluids. These results raise the following questions: (1) By which mechanisms did zircon form during Naxos metamorphism? (2) Is it possible to relate these scattered ages to metamorphic pressure–temperature conditions? These questions will be addressed through U–Pb geochronological studies associated with petrography and isotopic analysis. For this purpose, three samples have been selected in the metasedimentary sequence in the vicinity of the migmatitic core of the island (Fig. 1B). The samples are an amphibolite NA0180b, a calc-silicate gneiss NA01113b, and a metapelite NA0262b.

2. Analytical techniques

Elemental compositions of garnet and zircon were analysed with a CAMECA SX 100 electron microprobe at the Henri Poincaré University, Nancy. Acceleration voltage was 10 kV and beam current 10 nA for major minerals, 100 nA for zircon. The detection limits fall between 0.05 and 0.1% wt. for major elements and are reported in Table 3 for trace elements in zircon. Garnet zoning was imaged with a Hitachi 2500 scanning electron microscope (SEM).

For U–Pb and oxygen isotope measurements, zircon crystals were extracted from the 50–200 μm size fraction with heavy liquids and magnetic separation. Individual zircon grains were then handpicked and mounted in epoxy resin together with 91500 standard zircon grains. After polishing, all grains were examined in back-scattered electron microscopy and cathodoluminescence using a Philips XL30 SEM in order to characterise their internal texture. Zircon crystals were then chosen for in situ analyses on the basis of their internal texture, size and absence of inclusions. U–Pb analyses were performed with Cameca IMS1270 at CRPG-CNRS in Nancy using an O_2^- primary ion beam accelerated at 13 kV with an intensity of 10 nA (Deloule et al., 2002). Analytical data were corrected for instrumental fractionation using the 91500 zircon standard, dated at 1062.4 ± 0.4 Ma (Wiedenbeck et al., 1995). Corrections for common lead use the measured ^{204}Pb content and take into account the Stacey and Kramers (1975) lead evolution. Oxygen isotopic compositions in garnet and zircon were measured with the Cameca IMS1270 in Nancy using a Cs^+ primary ion beam accelerated at 10 kV with an intensity of 10 nA. The detection mode is multicollection in FC/FC mode. For zircon, instrumental mass fractionation was corrected using the 91500 zircon standard whose $\delta^{18}O$ value was measured at 10.09 ± 0.24‰ using BrF_5 extraction and gas source mass spectrometer at CRPG. Oxygen isotope measurements of garnet were performed on thin section. Standard grains were mounted on a separated polished section. In garnet, the instrumental mass fractionation is dependant on the elemental composition (Eiler et al., 1997). This matrix effect was corrected using a set of garnet standards of different elemental compositions following Vielzeuf et al. (2003). The standards used in this study were B114 ($\delta^{18}O$=9.3‰, France-Lanord et al., 1988; Vielzeuf et al., 2003), GrsSE ($\delta^{18}O$=3.8‰) and SpeSE ($\delta^{18}O$=5.4‰) (Elphick et al., 1985; Eiler et al., 1997), and UWG-2 ($\delta^{18}O$=5.8‰, Valley et al., 1995). For each garnet sample, three garnet standards with the most appropriate composition were chosen. In all cases (U–Pb and oxygen isotopic compositions), the size of the elliptical spot was ca. 20 × 15 μm. The errors reported for U–Pb and oxygen isotopic compositions are all at one sigma and take into account both internal (analytical) and external (standard reproducibility) errors. Error on oxygen isotope measurements in garnet is typically in the range of 0.2–0.5‰. Error on oxygen isotope measurements in zircon is between 0.4‰ and 1‰ because of the instability of the primary beam on zircon due to the size of the grains and their high relief. Photomicrographs of zircon were taken before

and after isotopic analysis in order to check the location of the analyses.

3. Samples description

Metabasite NA0180b was sampled in the higher levels of the kyanite–sillimanite transition zone (Va, Fig. 1B) defined by Jansen and Schuiling (1976). This zone is characterised by a peak temperature during M2 estimated at 500 °C (Wijbrans, 1985) and 620 °C (Jansen and Schuiling, 1976). Three successive paragenesis are recognised: (1) garnet+epidote+rutile; (2) garnet+hornblende+plagioclase+ilmenite, which is the dominant paragenesis; and (3) chlorite+titanite. Minerals rarely present equilibrium texture. Garnet crystals are strongly zoned (Table 1, Fig. 2): from core to rim, the spessartine component first decreases, and then increases, whereas Fe/(Fe+Mg) ratio decreases continuously. The grossular component presents a plateau in the core and then decreases towards the rim. This trend is interpreted as a growth zoning (Spear, 1993) and has been assigned to a "decompression-heating" path (Spear, 1993). Following this assumption, garnet cores must have grown at higher pressure and lower temperature than the rims. Nevertheless, due to the absence of relict minerals as inclusions, no pressure–temperature estimates could be made for this earlier growth. According to the observed garnet zoning in metabasite NA0180b, the paragenesis constituted by garnet rims and hornblende should be concomitant of the temperature peak. Taking previous studies on the metamorphic evolution of Naxos (Avigad, 1998; Jansen and Schuiling, 1976) into consideration, the pressure–temperature path followed by this sample is summarized on Fig. 3.

Table 1
EMP analyses (wt.% oxide) of garnet for samples NA0180b, NA01113b and NA0262b

Sample	NA0180b			NA01113b		NA0262b	
Domain	A, rim	B	C, core	Rim	Core	Rim	Core
SiO_2	37.7	36.75	37.59	38.37	37.6	37.73	38.09
Al_2O_3	20.82	19.83	19.79	21.01	20.91	21.47	21.63
FeO	17.35	30.31	21.04	14.04	14.49	24.32	27.12
MnO	15.25	2.85	11.18	13.34	9.93	3.61	2.37
MgO	2.5	1.48	0.97	1.59	2.05	2.62	3.15
CaO	7.64	8.35	10.45	10.19	12.34	10.78	8.93
Total	101.26	99.57	101.02	98.54	97.32	100.53	101.29
Formulae on the basis of 12 oxygens							
Si	2.98	2.99	3.01	3.08	3.03	2.96	2.97
Al	1.94	1.9	1.87	1.99	1.99	1.99	1.99
Fe^{2+}	1.15	2.06	1.41	0.94	0.98	1.51	1.71
Mn	1.02	0.2	0.76	0.91	0.68	0.24	0.16
Mg	0.29	0.18	0.12	0.19	0.25	0.31	0.37
Ca	0.65	0.73	0.9	0.88	1.07	0.91	0.75
End member proportions							
X_{pyrope}	0.09	0.06	0.04	0.07	0.08	0.1	0.12
$X_{almandine}$	0.37	0.65	0.44	0.32	0.33	0.52	0.58
$X_{spessartine}$	0.33	0.06	0.24	0.31	0.23	0.08	0.05
$X_{grossular}$	0.21	0.23	0.28	0.3	0.36	0.3	0.25

For garnet of sample NA0180b, the letters A, B, C refer to Fig. 2A.

Metasediments NA01113b and NA0262b was sampled in the sillimanite transition zone (Vb, Fig. 1B) defined by Jansen and Schuiling (1976), and is characterised by a peak temperature during M2 estimated between 560 °C (Wijbrans, 1985) and 660 °C (Jansen and Schuiling, 1976). Their *PT* path is summarised on Fig. 3.

Calcic gneiss NA01113b presents three main paragenesis: (1) epidote+garnet+K-feldspar+anorthite ± diopside (all minerals as relics), (2) scapolite+hornblende+titanite (oriented in the main foliation) and (3) chlorite+pyrite+calcite (retrogressive and concentrated in fractures). Garnet crystals are generally partly resorbed. They are almandine and grossular-rich (Table 1, Fig. 4, $X_{almandine} \approx 0.33$, $X_{grossular} \approx 0.36$). The slight zoning in the core is interpreted as a growth zoning partly homogenised during high temperature metamorphism (M2). The smaller garnet crystals (diameter lower than 200 μm) C12A and C12B show rims of 20–30 μm, richer in spessartine and with higher Fe/(Fe+Mg) ratio (Figs. 5A to C and 6). The increase of Fe/(Fe+Mg) ratio and spessartine component towards the margin in the smaller crystals supports the suggestion of retrogressive diffusion zoning at garnet margins during their partial resorption (Spear, 1993, p. 580).

Three paragenesis are observed in metapelite NA0262b: (1) kyanite+garnet occurring as porphyroblasts in the foliation, (2) biotite ± sillimanite, sillimanite, synchronous with the foliation, and (3) chlorite+calcite+titanite, retrogressive and localised in C-planes and in garnet fractures. Two types of garnet are observed: (i) as small crystals (up to

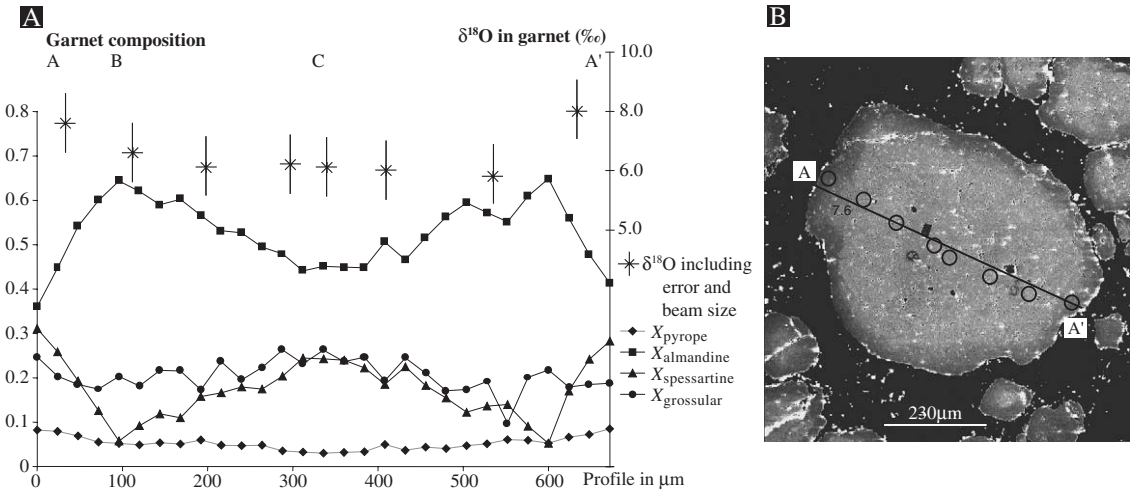

Fig. 2. $\delta^{18}O$ and major element composition of garnet from amphibolite NA0180b. Graph A represents the A–A′ profile in elemental composition and in $\delta^{18}O$ from the garnet shown on the BSE image B. A, B, C refer to compositional analyses shown in Table 1. Errors in $\delta^{18}O$ are ca. 1‰, and are represented on the graph by the vertical line. The size of the beam is ca. 25 µm, the width of the symbol. Black circles on BSE image B shows the location of the $\delta^{18}O$ analyses.

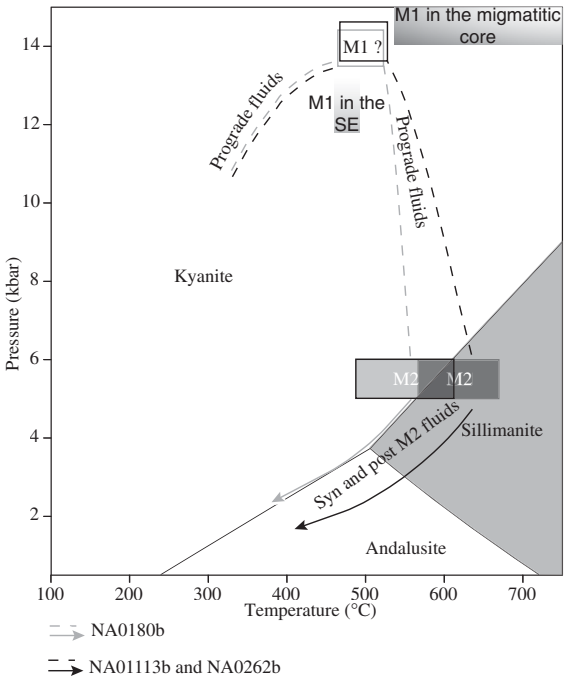

Fig. 3. Pressure–temperature paths for metabasite NA0180b and metasediments NA01113b and NA0262b (dashed and solid lines). Peak pressure and pressure–temperature path between M1 and M2 are based on calculations and estimates of pressure–temperature conditions in the southeast (vertical shaded rectangle) and in the core (horizontal shaded rectangle) of Naxos respectively from Avigad (1998).

500 µm in diameter, Fig. 5) in the foliation, and (ii) as large crystals (up to 5 mm in diameter, Fig. 6) in quartz and feldspar rich zones. In terms of major element composition, both types of garnet are almandine-rich ($X_{almandine} \approx 0.50$, Fig. 5, profiles B and D, and Fig. 6, profile D). Garnets are unzoned (Figs. 5 and 6) except on a thin rim of 30 µm on average for the small crystals (Table 1, Fig. 5, profiles B and D), where $X_{spessartine}$ increases, $X_{almandine}$ and X_{pyrope} decrease and Fe/(Fe+Mg) ratio increases. The flat shape of the profile in the core of garnet crystals, as well as the increase in Fe/(Fe+Mg) ratio in the rim, suggest retrogressive diffusive zoning resulting from Fe, Mg, Mn exchange between neighbouring minerals (0.1 to 0.5 wt.% of MnO in biotite, 0.5 to 2 wt.% of MnO in ilmenite) rather than growth zoning.

As described above, garnet in amphibolite NA0180b, located in the kyanite–sillimanite transitional zone (500–620 °C) has preserved growth zoning and records the polyphased history observed in metamorphic rocks from Naxos. By contrast, samples NA01113b and NA0262b, located in the sillimanite zone, do not show such zoning. In this zone, the temperature was estimated between 560 and 660 °C during M2 metamorphism (Jansen, 1973; Jansen and Schuiling, 1976). This range in temperature

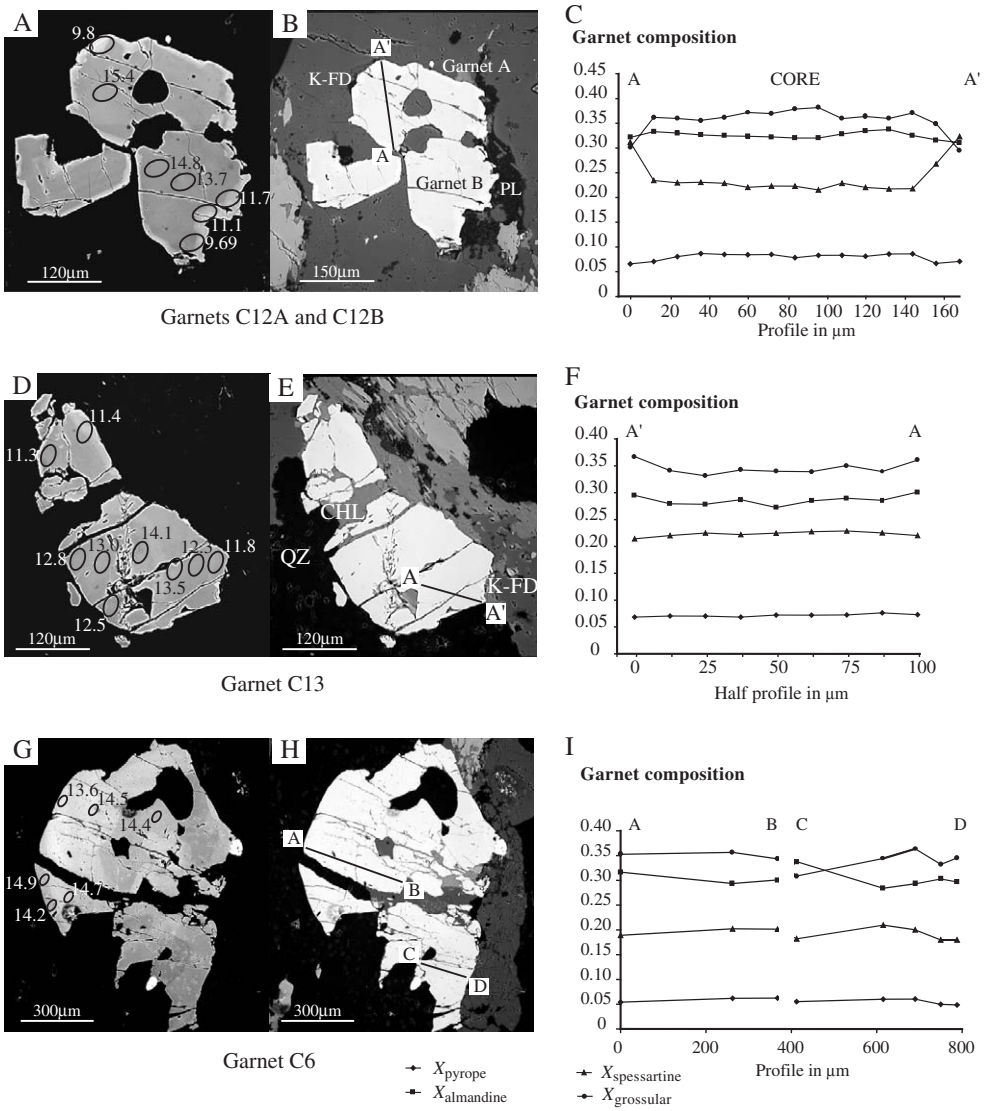

Fig. 4. $\delta^{18}O$ and elemental compositions measured in garnets from sample NA01113b. The pictures A, B, D, E, G, and H are BSE images. The minerals in the vicinity of garnet are orthoclase (K-FD), plagioclase (PL), quartz (QZ) and chlorite (CHL). The black ellipses show the location of $\delta^{18}O$ analyses. The $\delta^{18}O$ values measured are reported in ‰. The error on $\delta^{18}O$ values is ca. 1‰. BSE images A and B represent garnet C12A and C12B. A′–A compositional profile is represented on graph C. BSE photomicrographs D and E represent garnet C13. A′–A compositional profile is represented on graph F. BSE photomicrographs G and H represent garnet C6. A–B and C–D compositional profiles are shown on graph I.

overlaps or exceeds the closure temperature for major elements (Ca, Fe, Mg, Mn) in garnet which is 550–650 °C when calculated with the diffusion data of Cygan and Lasaga (1985) and Chakraborty and Ganguly (1992), using a cooling rate of 10–30 °C/Ma and a garnet radius of 100–150 µm.

4. Oxygen isotope in garnet

Oxygen isotope analyses for garnet crystals of metabasite NA0180b, calcic gneiss NA01113b and metapelite NA0262b are reported in Table 2 and Figs. 4–6.

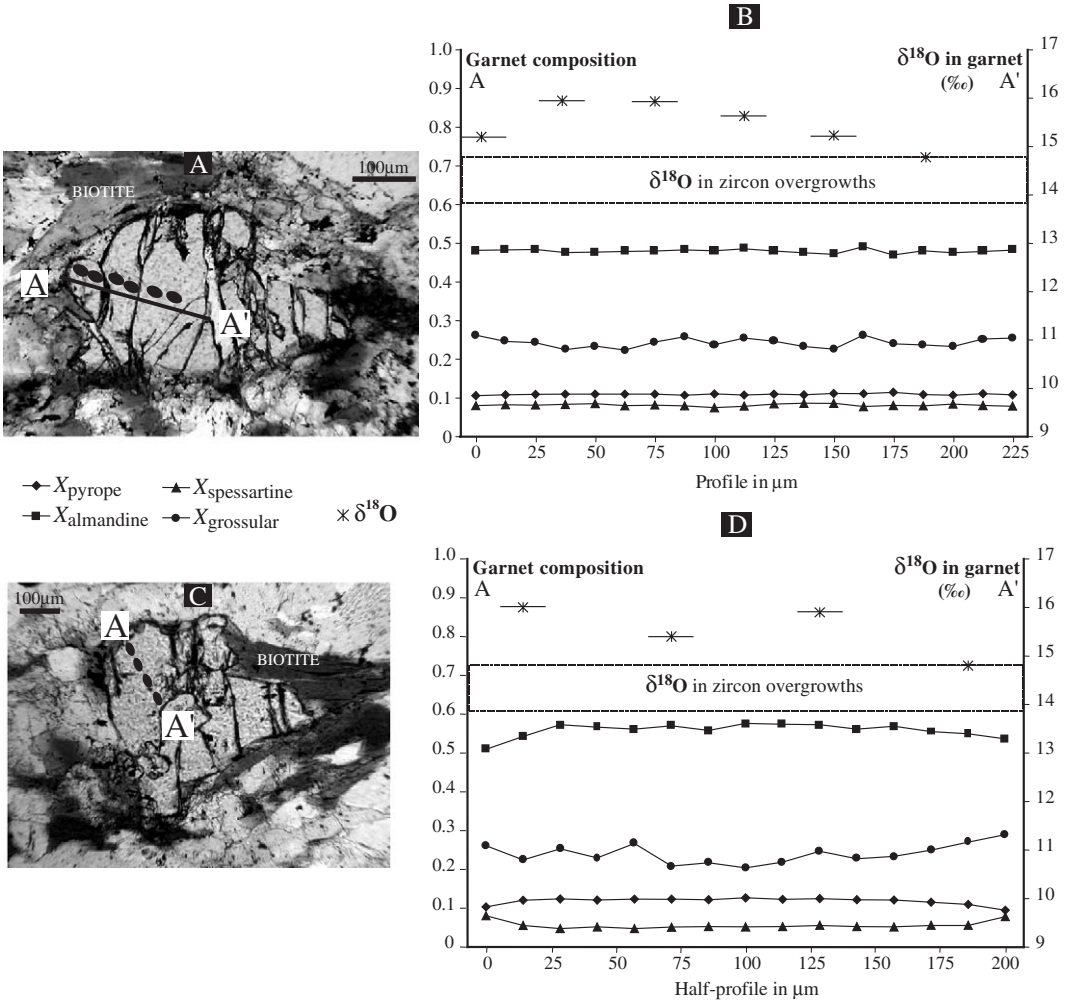

Fig. 5. $\delta^{18}O$ and elemental compositions measured in small garnet crystals from sample NA0262b. Graph B represents the A–A′ $\delta^{18}O$ and compositional profile of the garnet shown in thin section in microphotograph A. Graph D represents the A–A′ $\delta^{18}O$ and compositional profile of the garnet shown in thin section in microphotograph C. The analytical error on $\delta^{18}O$ values is in the size of the symbol, and is ca. 0.2‰. The size of the beam is ca. 25 μm, the width of the symbol.

4.1. Metabasite NA0180b

Oxygen isotope composition was analysed along four traverses in garnet crystals from amphibolite NA0180b (one representative traverse is shown on Fig. 2A and 2B). Garnet crystals were chosen in contact with different minerals (hornblendes grown at peak temperature, and retrogressive phyllosilicates) in order to estimate the effect of the neighbouring minerals on $\delta^{18}O$ value measured in garnet crystals. Irrespective of the mineral in the vicinity of the analysed garnet, $\delta^{18}O$ increases from the core (Fig. 2A, 6.3 ± 0.6‰, $n=4$) towards a 50 μm thick rim (8.1 ± 1.6‰, $n=4$). This increase of 2‰ can be explained either by growth zoning or by diffusive zoning, in closed or open system. Either garnet rims grew with a $\delta^{18}O$ similar to that of garnet cores and $\delta^{18}O$ increased later due to retrogressive diffusional exchange with surrounding minerals or fluids, or they grew with high $\delta^{18}O$ at equilibrium during M2. Making the assumption of a maximum characteristic time for diffusion of 5 Ma, and considering

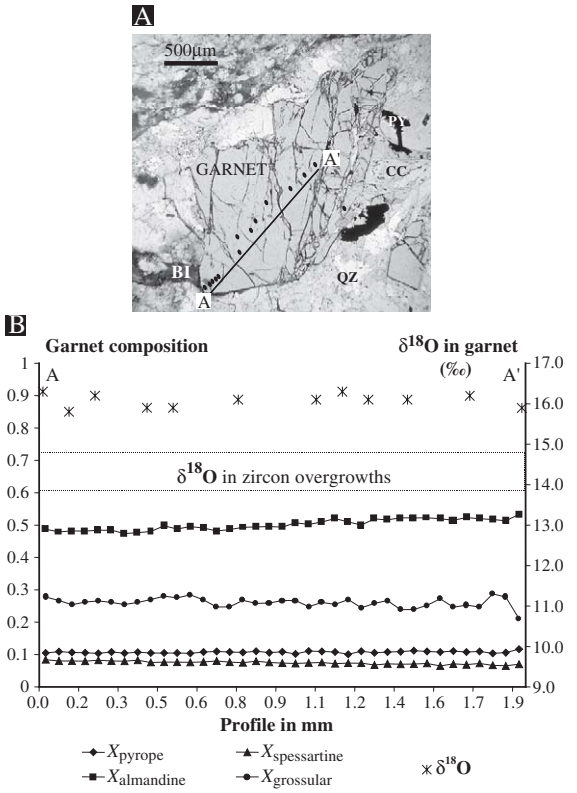

Fig. 6. $\delta^{18}O$ and elemental compositions measured in large garnet crystals from sample NA0262b. Picture A shows a thin section photomicrograph of the garnet crystals analysed for elemental and $\delta^{18}O$ compositions along the half traverse A–A′. Neighbouring minerals are pyrite (PY), calcite (CC), quartz (QZ) and biotite (BI). Graph B is the $\delta^{18}O$ and elemental compositions A′–A half profile in the garnet from picture A. The size of the beam and the analytical error on $\delta^{18}O$ values (ca.± 0.2‰) are in the size of the symbol.

diffusion data for oxygen from Zheng and Fu (1998), the characteristic length for diffusion is less than 10 µm at a temperature of 560 °C (average temperature during M2 in the kyanite–sillimanite transition zone) which conflicts with the observed 50 µm zoning. The hypothesis of a diffusive zoning of $\delta^{18}O$ can therefore be ruled out. As an alternative, oxygen isotope composition can be explained by growth zoning either in closed or in open system, in equilibrium with the mineral in the vicinity that is generally hornblende. As garnet rims and hornblende are in equilibrium and form the main high temperature paragenesis, the increase in $\delta^{18}O$ on the garnet rim is interpreted as coincident with the M2 metamorphic event.

4.2. Calcic gneiss NA01113b

$\delta^{18}O$ was measured in four garnet crystals from calcic gneiss NA01113b (Fig. 4). The main minerals in their vicinity are orthoclase, quartz and plagioclase. $\delta^{18}O$ in garnet crystals C12A, C12B (Fig. 4A) and C13 (Fig. 4D) strongly decreases from core (14.4 ± 0.7‰, $n=3$) to rim (11.4 ± 1.1‰, $n=3$). Garnet C6 displays a constant $\delta^{18}O$ value of 14.4 ± 0.5‰ (Fig. 4G). The $\delta^{18}O$ calculated for the fluid in equilibrium with garnet (using partition coefficients from Zheng, 1993) are between ca. 17‰ (for garnet cores) and ca. 14‰ (for garnet rims), considering a temperature range of 400–670 °C for prograde growth. This range of values corresponds to the signature of prograde fluids ($12‰ < \delta^{18}O < 16‰$, Baker et al., 1989), which suggests that garnet grew during the prograde

Table 2
Oxygen isotope analyses for metabasite NA0180b and metapelite NA0262b (oxygen isotopes analyses for calcic gneiss are reported on Fig. 4)

NA0262b			NA0180b		
Profile in mm	$\delta^{18}O$ (‰)	± σ (‰)	Profile in µm	$\delta^{18}O$ (‰)	± σ (‰)
Figure 6			*Figure 2*		
0.000	16.3	0.2	33	7.6	1.0
0.104	15.8	0.2	112	6.6	1.0
0.208	16.2	0.2	198	6.1	1.0
0.416	15.9	0.2	297	6.2	1.0
0.520	15.9	0.2	340	6.1	1.0
0.780	16.1	0.2	409	6.0	1.0
1.092	16.1	0.2	535	5.8	1.0
1.196	16.3	0.2	634	8.0	1.0
1.300	16.1	0.2			
1.456	16.1	0.2			
1.664	16.1	0.2			
1.872	15.8	0.2			
Figure 5 A and B					
0	15.2	0.2			
36	15.8	0.2			
72	15.8	0.2			
108	15.5	0.2			
144	15.1	0.2			
180	14.8	0.2			
Figure 5 C and D					
14	16.0	0.2			
70	15.4	0.2			
126	15.9	0.2			
182	14.8	0.2			

metamorphism. The decrease in $\delta^{18}O$ from 14.4‰ in cores to 11.4‰ in rims observed in garnet crystals C12B, C12C and C13 can be explained by either garnet growth in equilibrium with prograde fluids or diffusion from late M2 fluids characterised by a low $\delta^{18}O$ value ($\delta^{18}O < 10‰$, Baker et al., 1989).

4.3. Metapelite NA0162

Three traverses were analysed in metapelite NA0262b. In two small garnet crystals (Fig. 5A to D), $\delta^{18}O$ increases from the cores ($14.8 \pm 0.2‰$) towards the rims ($15.7 \pm 0.5‰$). As observed in garnet cores from the calcic gneiss, the $\delta^{18}O$ calculated for the fluid in equilibrium with garnet matches those of Naxos prograde fluids. The slight increase in $\delta^{18}O$ values from core to rim in garnet is not consistent with late partial re-equilibration with retrogressive fluids, since those are characterised by lower $\delta^{18}O$ signature ($\delta^{18}O < 10‰$, Baker et al., 1989). It is best explained by the temperature increase during mineral growth, which can readily account for the observed variation in $\delta^{18}O$ of ca.1‰. In the large garnet (Fig. 6A, D), $\delta^{18}O$ does not show any marked variation ($16.1 \pm 0.3‰$ in average).

5. Zircon study: morphology, U–Pb dating and oxygen isotope

5.1. Internal texture

Cathodoluminescence and/or back-scattered electron images of zircon crystals from the three samples are shown in Figs. 7 and 8, with a schematic diagram of the internal texture. In the three samples, zircon crystals are characterized by metamorphic zones surrounding cores. In the following, the word "rim" is used by default instead of overgrowth whenever it could not be proved that zircon was newly formed. Of all analysed samples, zircon crystals from metabasite NA0180b preserve the most complete history. They are characterised by a core truncated by two rims denoted as A and B (Fig. 7). The core is oscillatory zoned and rich in apatite inclusions. Both rims are slightly zoned. The first rim A is highly luminescent in cathodoluminescence, and separated from the core by a transitional zone that is dark in cathodoluminescence (Fig. 7). The second rim B is not always present and is thinner than rim A. It is dark in cathodoluminescence. The different parts of the zircon are chemically distinct. The cores are richer in Y, P, Yb, U, Th, than the rims and HfO_2 is below 1.2 wt.% (Table 3). Th/U ratio is greater than 0.14 (0.14–1.14, Table 4). In contrast, the rims have Th/U ratios lower than 0.1. Th/U ratio (Table 4) and HfO_2 content (Table 3) are higher in A (ca. 0.020 and 1.6 wt.%) than in B (ca. 0.002 and 1.4 wt.%).

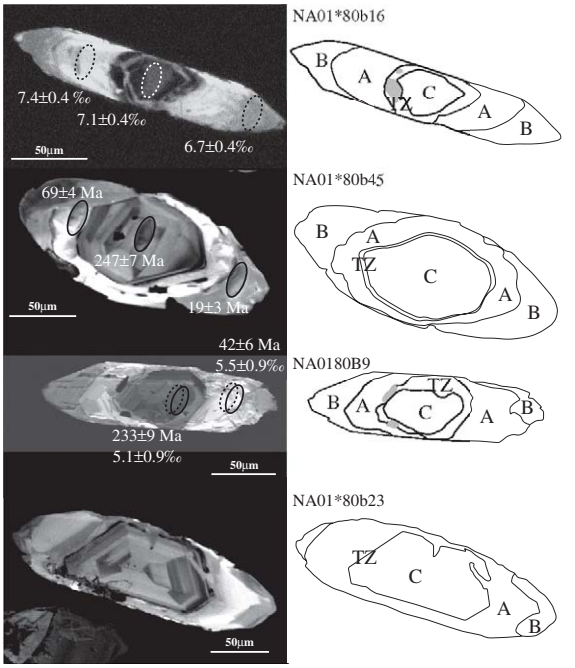

Fig. 7. Cathodoluminescence images and schematic sketches of internal textures of typical zircon from amphibolite NA0180b. Analytical spots for U–Pb dating (solid line ellipse) and for oxygen isotopes (doted line ellipses) are reported with the corresponding ages and $\delta^{18}O$. The name of each zircon is: name of the sample and name of the zircon. C: magmatic core, A: first rim, B: second rim, TZ: transitional zone between the magmatic core and the first metamorphic rim. Shaded areas represent inclusions.

Zircon from metapelite NA0262b (Fig. 8A to D) and calcic gneiss NA01113b (Fig. 8E to H) do not present regular shapes as observed in amphibolite NA0180b. They present cores mantled by a single rim (A′). Morphological heterogeneity of the cores suggests a detrital origin. The contact between the core and the rim is blurred and dark in cathodoluminescence. A′ is generally heterogeneous and presents irregular zoning (Fig. 8B). The metamorphic rims are

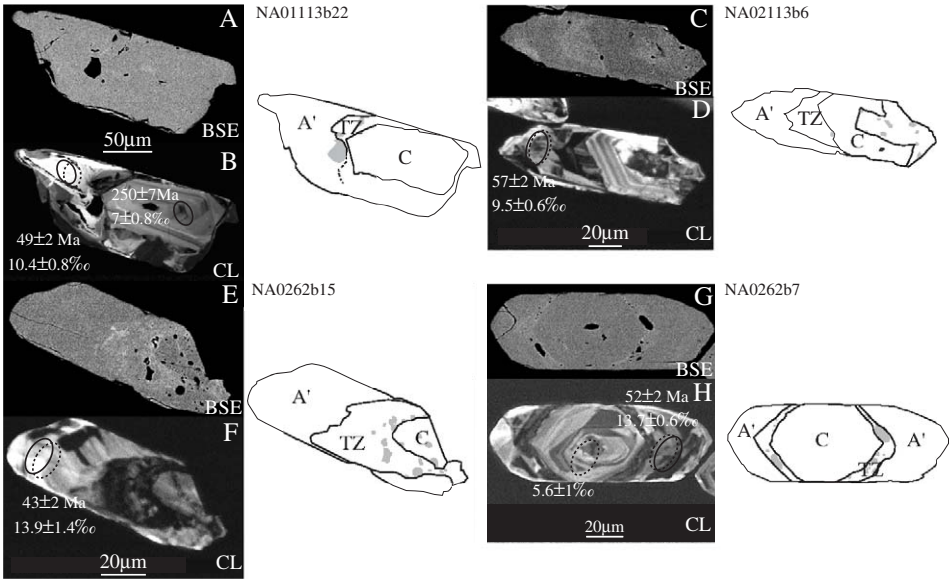

Fig. 8. Cathodoluminescence (CL), back-scattered electron (BSE) images, and schematic sketches of internal textures of typical zircon from metasediments NA01113b (A–D) and NA0262b (E–H). Analytical spots for U–Pb dating (solid line ellipses) and for oxygen isotopes (doted line ellipses) are reported with corresponding ages and $\delta^{18}O$. U–Pb and oxygen analyses are in Table 6. The name of each zircon is: name of the sample and name of the zircon. C: magmatic core, A′: metamorphic overgrowth, TZ: transitional zone between the magmatic core and the metamorphic overgrowth. Shaded areas represent inclusions.

characterised by high Hf, low Y content (Table 5) and low Th/U ratios (Table 6, between 0.001 and 0.005).

5.2. U–Pb dating

Each domain of the selected zircon was dated individually (Tables 4 and 6). The young age of the metamorphic events associated with the low U contents (from 700 ppm down to less than 10 ppm) induces very low radiogenic Pb contents, below 10 ppm in most cases. These low Pb contents result in large errors on the calculated ages, especially the ^{207}Pb–^{235}U ages. Accordingly, ^{207}Pb–^{235} ages and associated apparent discordance are not always meaningful.

In sample NA0180b, three different age groups (Table 4, Fig. 9A) correspond to the three domains (the core and the metamorphic rims A and B, Fig. 7). The ages of the cores are nearly concordant, between 200 and 270 Ma. With respect to the zoning and the chemical composition observed in the zircon core, they are interpreted as dating their magmatic crystallisation. The A rims yield ages between 42 and 69 Ma, that correspond to the Ar/Ar and K/Ar ages of blueschist relics in the south of Naxos (Andriessen et al., 1979; Wijbrans and McDougall, 1986; Andriessen, 1991), with two subgroups at 44 ± 3 Ma ($n=4$) and 55 ± 6 Ma ($n=5$). Lastly, B-rims are dated between 14 and 19 Ma which is consistent with U–Pb dating of zircon from migmatite (Keay et al., 2001; Keay, 1998). In samples NA0262b and NA01113b (Table 6, Fig. 8), ages in the cores are highly variable (150 to 1900 Ma), which confirms their detrital origin. The metamorphic rims are constrained at between 41 and 57 Ma (with the exception of one single discordant age of 34 Ma), with two subgroups aged at 44 ± 3 Ma ($n=4$) and 54 ± 6 Ma ($n=4$) (Fig. 9B). No Miocene age was measured in these two samples. Some of the measured ages are concordant, which allows the 44 ± 3 and 54 ± 6 Ma ages to be interpreted as metamorphic crystallisation ages.

5.3. Oxygen isotope

Oxygen isotope compositions were analysed in rims and cores of the zircon described above. $\delta^{18}O$ values measured in zircon cores and rims A of amphibolite NA0180b are plotted on the Fig. 7, and reported in Tables 4 and 7. $\delta^{18}O$ values measured in the core (from

Table 3
Examples of EMP analyses (wt.% oxide) performed on zircon A rim, B rim and core in sample NA0180b

Metabasite NA0180b														
Domain	DL	Rim B	Rim B	Rim B	Rim A	Rim A	Rim A	Core	Rim B	Rim B	Rim A	Core	Rim	Core
label		80b36-1	80b36-2	80b36-3	80b36-5	80b36-6	80b36-7	80b36-12	80B46-1	80B46-3	80B46-3	80B46-4	A 80B23-4	80B23-8
SiO_2	0.5	30.78	31.19	30.53	31.05	31.2	30.3	31.12	31.39	32.05	30.5	31.6	31.22	30.84
P_2O_5	0.02	0.06	0.06	0.05	0.03	0.03	–	0.07	0.08	0.06	0.06	0.07	–	–
Y_2O_3	0.02	–	–	–	–	–	–	0.19	–	–	–	0.19	–	0.4
ZrO_2	0.5	63.51	63.31	63.43	63.74	63.56	63.48	64.37	65.79	67.26	64.29	66.6	64.73	64.93
Yb_2O_3	0.06	–	–	–	–	–	–	0.06	–	–	–	0.06	–	0.15
HfO_2	0.02	1.38	1.41	1.47	1.58	1.57	1.56	0.93	1.33	1.36	1.71	1.39	1.55	0.94
Total		95.73	95.97	95.48	96.39	96.35	95.34	96.73	98.59	100.76	96.61	99.94	97.57	97.25

Note: All samples are prefixed by NA01, DL: detection limit, "–": below detection limit.

4.8‰ to 7.3‰, 6.2 ± 0.8‰ on average) are in the range of $\delta^{18}O$ values described in mafic rocks (5–6‰, Eiler et al., 2000). $\delta^{18}O$ values measured in the A rims are between 4.7‰ and 7.4‰ (7 ± 1‰ on average, $n=7$). Fig. 10 compares $\delta^{18}O$ values measured in the core and in the first rim of each zircon and provides evidence that these values are almost similar. Four analyses only were performed in the second rim B (Fig. 7 and Tables 4 and 7), because this last rim is rarely large enough to be measured. The overgrowth B is characterised by $\delta^{18}O$ values scattered between 6.7‰ and 9‰ (7.8 ± 1.8‰ on average, $n=4$). Even if $\delta^{18}O$ seems to increase in between rim A and rim B, this trend is not verified by zircon 80b16 (Table 7 and Fig. 7). This will be discussed below together with garnet oxygen isotope data. Zircon metamorphic overgrowths in calcic gneiss NA01113b and in metapelite NA0262b present higher $\delta^{18}O$ values compared to the cores (Tables 6 and 7, Fig. 8). In calcic gneiss NA01113b, $\delta^{18}O$ measured in the core is between 4.9‰ and 7‰ (6.1 ± 1.5‰ in average for $n=4$) whereas overgrowths are characterised by $\delta^{18}O$ of 11.8 ± 1.4‰ (average for $n=7$). In metapelite NA0262b, $\delta^{18}O$ measured in the core scatters from 5‰ to 10‰ ($n=6$) and $\delta^{18}O$ measured in the overgrowths is between 13.7‰ and 15.5‰ (in average 14.2 ± 0.5‰ with $n=8$).

6. Discussion

6.1. Zircon growth mechanisms

In the three samples, metamorphic zircon appears solely as rims around relict magmatic cores or around detrital grains. The oscillatory zoning of the cores is truncated by the metamorphic rims with either blurred or sharp, sometimes lobed, contacts, which were interpreted as a sign of recrystallisation by Pidgeon (1992) and Hoskin and Black (2000). Moreover, the contact between the metamorphic rim and the core is characterized by a bright zone in BSE and dark in cathodoluminescence (Fig. 8G). This feature was interpreted as a zone concentrating impurities during zircon recrystallisation (Corfu et al., 2003; Pidgeon et al., 1998). Zircon internal textures are therefore indicative that zircon rims observed at the contact with relict or detrital cores in the three samples formed by their recrystallisation. Nevertheless, in the absence of

Table 4
U–Pb isotopic data on zircon from sample NA0180b. Oxygen isotope measurements are also reported when performed on the same zircon as U–Pb analyses

Name of UPb analysis	Name of $\delta^{18}O$ analysis	Domain	Contents (ppm)				Measured	% Pbc	Corrected ratios						Ages (Ma)				$\delta^{18}O$ (‰)	$\pm\sigma$ (‰)
			Pb	U	Th	Th/U	$^{204}Pb/^{206}Pb$		$^{207}Pb/^{206}Pb$	$\pm\sigma$	$^{206}Pb/^{238}U$	$\pm\sigma$	$^{207}Pb/^{235}U$	$\pm\sigma$	$^{206}Pb/^{238}U$	$\pm\sigma$	$^{207}Pb/^{235}U$	$\pm\sigma$		
80b23-2		Core	8.72	241	147.46	0.6126	0.00039	0.4	0.0538	0.0008	0.0421	0.0027	0.3128	0.0206	266	17	276	16		
80b38-2		Rim A	0.27	37	0.20	0.0054	0.01818	21.5			0.0085	0.0009			55	6				
80b2-1	80b-2-1	Core	11.64	351	399.21	1.1380	0.00167	2.9	0.0586	0.0038	0.0386	0.0015	0.3122	0.0234	244	9	276	18	5.2	0.4
80b38-2b		Rim A	3.79	613	13.58	0.0221	0.00669				0.0072	0.0008			46	5				
80b4-2b	80b-4-1	Core	6.82	224	125.74	0.5602	0.00456	8.12	0.055	0.0051	0.0354	0.0014	0.2681	0.0271	224	9	241	22	4.8	0.5
	80b-4-2	Rim A																	4.7	0.5
80b6-1b	80b6-2	Rim A	0.11	14	1.44	0.1032	0.01107	17.5			0.009	0.0009			58	5			7.4	0.4
80b6-2b	80b6-1	Core	12.88	364	222.08	0.6096	0.00060	1.1	0.0504	0.0006	0.0412	0.0015	0.2858	0.0111	260	9	255	9	6.6	0.4
80b6-3b		Rim B	0.09	43	0.16	0.0038	0.01542	23.6			0.0024	0.0004			16	2				
80b9-2	80b9-1	Core	0.70	656	436.23	0.6652	0.00065	1.2			0.0368	0.0014			233	9			5.1	0.9
80b9-3	80b9-2	Rim A	20.73	33	0.79	0.0244	0.01363	16.1	0.0509	0.0008	0.0065	0.0009	0.2581	0.0105	42	6	155	43	5.5	0.9
80b25-2		Rim A	0.03	16	0.25	0.0162	0.00955	17.1	0.007	0.0003	0.0083	0.0004			53	2				
80b26-4		Core	0.10	184	26.53	0.1441	0.00266	6.7	0.0031	0.0001	0.0396	0.001			250	6				
80b30-5	80b30-2	Core	0.28	151	22.34	0.1482	0.00102	2.5			0.0405	0.0008			256	5			6.5	1
80b38-5		Rim B	5.24	19	0.01	0.0003	0.02759	34.1			0.0024	0.0003			15	2				
*80b33-2		Rim B	0.30	28	0.01	0.0003	0.03933	65.0			0.0022	0.0029			14	19				
*80b33-3		Rim A	0.05	6	0.01	0.0012	0.02381	33.5			0.0062	0.0018			40	12				
*80b33-4		Core	0.03	115	27.34	0.2372	0.00039	0.6	0.0515	0.0016	0.0324	0.001	0.2304	0.0101	206	6	211	8		
*80b27-1		Rim A	3.21	8	0.03	0.0035	0.01292	7.5	0.2083	0.0536	0.0069	0.0007	0.1985	0.0547	44	4	184	45		
*80b27-2		Core	0.05	321	105.17	0.3272	0.00017	0.3	0.0512	0.0008	0.0401	0.0013	0.2834	0.0101	254	8	253	8		
*80b45-1		Rim B	11.08	15	0.01	0.0010	0.01536	16.3	0.1119	0.064.	0.003	0.0004			19	3				
*80b45-2		Rim A	0.04	9	0.25	0.0292	0.00684	7.0			0.0107	0.0006	0.1141	0.0279	69	4	110	25		
*80b45-3		Core	0.08	107	36.38	0.3405	0.00026	0.3	0.0509	0.0006	0.039	0.0011	0.2739	0.0085	247	7	246	7		
*80b10-1		Rim A	0.14	30	1.14	0.0376	0.00514	7.7			0.0099	0.0009			63	6				
*80b10-2		Core	0.26	93	15.23	0.1636	0.00689	12.4	0.0535	0.0088	0.0392	0.0016	0.2888	0.049	248	10	258	38		

Note: %Pbc is the percent of common lead in the ^{206}Pb intensity as determined by measured ^{204}Pb.

Note: all samples are prefixed by NA01 (80). The name of isotopic analyses must be read as: name of the sample, naame of zircon and name of the analyses.

*: same sample as NA0180b, but zircon crystals are on a second polished section.

Oxygen isotope data in the second column were measured at the same place (zircon and domain) as the U–Pb dating.

σ on $\delta^{18}O$ value take into account the external and internal errors.

Table 5
Examples of EMP analyses (wt.% oxide) performed on zircon rims and cores in sample NA01113b

Calcic gneiss NA01113b							Metapelite NA0262b					
Domain	Rim	Rim	Rim	Rim	Core	Core	Domain	Rim	Rim	Core	Core	Core
Label	113b22-1	113b22-2	113b22-3	113b22-4	113b22-5	113b22-6	Label	62b7-1	62b7-2	62b7-4	62b7-5	62b7-6
SiO_2	31.66	32.72	32.4	32.7	32.44	32.64	SiO_2	32.5	32.15	32.25	31.73	31.77
P_2O_5	0.04	0.03	0.02	0.05	0.03	0.04	P_2O_5	0.08	0.06	0.08	0.11	0.12
Y_2O_3	–	–	0.02	–	0.38	0.36	Y_2O_3	–	0.02	–	0.05	0.05
ZrO_2	65.11	66.48	65.92	66.35	66.74	66.74	ZrO_2	67.43	65.93	66.29	66.46	66.18
Yb_2O_3	–	–	–	–	0.12	0.13	Yb_2O_3	–	0.11	–	0.06	–
HfO_2	1.47	1.6	1.59	1.55	1.00	1.29	HfO_2	1.59	1.63	1.39	1.32	1.12
Total	98.28	100.83	99.95	100.65	100.71	101.2	Total	101.6	99.9	100.01	99.73	99.24

Note: All samples are prefixed by NA01 (calcic gneiss) or NA02 (metapelite), DL: detection limit, "–": below detection limit.

oscillatory ghost zoning inside the metamorphic domain (Hoskin and Black, 2000), dissolution–recrystallisation cannot be distinguished from a solid-state recrystallisation on the sole basis of the morphological criteria. In sample NA0180b, in each zircon, the $\delta^{18}O$ in the first (A) metamorphic rim is similar to the $\delta^{18}O$ measured in the relict core. Moreover, the $\delta^{18}O$ varies from one zircon crystal to another. If isotopic equilibrium was achieved at the rock scale during metamorphism, the same $\delta^{18}O$ value should be measured in all the rims, independent of the value of the corresponding core. $\delta^{18}O$ characteristics indicate that A rims formed in a closed system with regard to the $\delta^{18}O$ at the mineral scale. This is consistent with the formation of zircon metamorphic rims by solid-state recrystallisation from relict zircon. The obliteration of the magmatic texture in the A rims is related to the mobility of the impurities during metamorphism (Hoskin and Black, 2000). The decrease in Y, P, Yb, U, Th and Pb contents between zircon cores and rims, and the resetting of the U–Pb chronometers are evidence of this mobility.

In metasediments NA0262b and NA01113b, $\delta^{18}O$ values measured in the rims are significantly different from those measured in the cores in each zircon crystal. This indicates that recrystallisation of detrital zircon occurred in an open system at the mineral scale with regard to oxygen. Zircon rims formed either by solid state recrystallisation or by dissolution–recrystallisation. In the former case, high temperature (560–660 °C) and fluid-rich compositions may have been sufficient to allow diffusive exchange of oxygen isotopes between zircon rims (25–50 μm) and the surrounding matrix (Cherniak and Watson, 2003; Zheng and Fu, 1998). However, both the presence of well marked internal zoning in zircon overgrowths and their isotopic homogeneity support the second hypothesis.

The sole sample where two metamorphic rims are observed is the metabasite NA0180b. The contact between the first (A) and second (B) rims can be gradual or sharp. The internal texture of the B rims can be concordant or not with the A rims. When internal textures are present in the first rim, they are not observed as ghost zonings in the second, whatever the type of contact. The internal textures cannot therefore be interpreted in terms of growth mechanisms. $\delta^{18}O$ values measured in the B rims are not equal to those of the relict cores, and are higher than in the first rims (A). Formation of B zircon rims has therefore occurred when the system was open to oxygen exchange.

6.2. Linking zircon to garnet growth with oxygen isotopes

In sample NA0180b, the A rims preserved the $\delta^{18}O$ value of the zircon cores during solid-state recrystallisation. Therefore even if garnet and zircon crystals grew at the same time, they cannot have been in isotopic equilibrium during their formation. In this case, oxygen isotopes are useless for relating garnet and zircon growth. If it can be shown that metamorphic zircon formed in an open system at the mineral scale for oxygen, the comparison between $\delta^{18}O$ values of zircon and garnet is possible. This is the case in B zircon rims of sample NA0180b as well as in zircon overgrowths in samples NA01113b and NA0262b.

Table 6
U–Pb isotopic data on zircon from samples NA0262b and NA01113b

Name of U–Pb analysis	Name of $\delta^{18}O$ analysis	Domain	Contents (ppm)				Measured	% Pbc	Corrected ratios						Ages (Ma)				$\delta^{18}O$ (‰)	$\pm\sigma$ (‰)
			Pb	U	Th	Th/U	$^{204}Pb/^{206}Pb$		$^{207}Pb/^{206}Pb$	$\pm\sigma$	$^{206}Pb/^{238}U$	$\pm\sigma$	$^{207}Pb/^{235}U$	$\pm\sigma$	$^{206}Pb/^{238}U$	$\pm\sigma$	$^{207}Pb/^{235}U$	$\pm\sigma$		
NA0262b																				
62b15-1	62b15-1	Rim	0.83	142	0.15	0.0011	0.0067	11.1			0.0068	0.0003			43	2			13.9	1.4
	62b15-2	Rim																	15.5	1.4
62b20-2		Core	5.79	45	5.2	0.1166	0.0002	0.2	0.0627	0.0005	0.1511	0.0043	1.3072	0.0385	907	24	849	17	10.7	0.6
62b7-1	62b7-1	Rim	2.72	392	0.38	0.001	0.001		0.0432	0.0018	0.0081	0.0002	0.0482	0.0025	52	2	48	2	13.7	0.6
	62b7-2	Core																	5.4	0.6
62b6-1	62b6-1	Rim	1.62	270	0.53	0.002	0.0054				0.007	0.0005			45	3			14.7	1.4
62b6-2	62b6-2	Core	3.27	100	38.55	0.3864	0.0002	0.4	0.0465	0.0008	0.0382	0.0012	0.2449	0.0089	242	8	222	7	9.6	1.4
62b14-1	62b14-1	Rim	5.34	726	0.66	0.0009	0.0008		0.0415	0.0012	0.0086	0.0003	0.0489	0.0022	55	2	48	2	15.0	1.4
62b14-2	62b14-2	Core	17.53	60	11.78	0.1969	0.0002	0.2	0.1292	0.0005	0.3409	0.0107	6.0718	0.1911	1891	51	1986	27	8.2	1.4
NA01113b																				
113b36-1		Rim	1.07	235	0.55	0.0023	0.0038	5.3	0.0316	0.0046	0.0053	0.0001	0.023	0.0034	34.0	0.4	23	3		
113b35-1		Rim	1.09	200	0.5	0.0025	0.0022	2.9	0.0353	0.0024	0.0064	0.0001	0.031	0.0021	40.8	0.4	31	2		
113b35-2		Core	6.16	181	45.17	0.2496	0.0003	0.5	0.0482	0.0005	0.0396	0.0003	0.2632	0.0038	250	2	237	3		
113b38-1		Rim	1.31	213	1.18	0.0055	0.0012	1.4	0.047	0.0012	0.0071	0.0001	0.0462	0.0012	45.9	0.4	46	1		
113b22-1	113b22-r	Rim	1.31	47	0.42	0.1116	0.0011	4.5	0.0512	0.009	0.0077	0.0004	0.054	0.0098	49	2	53	9	10.4	0.8
113b22-2	113b22-c	Core	2.37	70	0.03	0.2028	0.0007	1.0	0.0463	0.0017	0.0396	0.0012	0.253	0.0118	250	7	229	10	7.0	0.8
113b5-1	113b5-2	Rim	0.98	162	0.99	0.001	0.0044	7.6	0.0346	0.0091	0.007	0.0003	0.0334	0.0088	45	2	33	9	13.0	0.6
113b6-2	113b6-1	Rim	4.99	656	0.09	0.0147	0.0006	1.1	0.0444	0.0008	0.0089	0.0003	0.0542	0.0019	57	2	54	2	9.5	0.6

Note: %Pbc ids the percent of common lead in the ^{206}Pb intensity as determined by measured ^{204}Pb.
Note: All samples are prefixed by NA01 (113b) or NA02 (62b). The name of isotopic analyses must be read as: name oft the sample, name of zircon and name of the analyses.
Oxygen isotope data in the second column were measured at the same place (zircon and domain) than the U–Pb dating.
σ on $\delta^{18}O$ value take into account the external and internal errors.

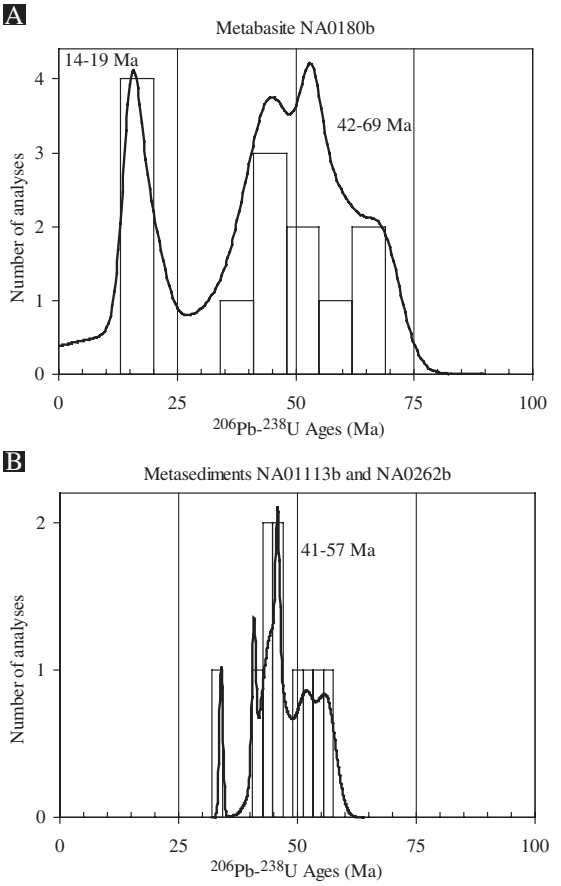

Fig. 9. Cumulative probability (thick black curve) and histogram of frequency distribution of the ^{238}U–^{206}Pb ages obtained on zircon from metabasite NA0180b (A) and from metasediments NA01113b and NA0262b (B).

In sample NA0180b, $\delta^{18}O$ values measured in zircon metamorphic overgrowths B (7.8 ± 1.8‰) are similar on average to those measured in garnet rims (8.1 ± 1.6‰). Given the absence of oxygen fractionation between garnet and zircon (Zheng, 1993), it supports the contemporaneous growth of garnet rims and zircon B rims. U–Pb ages at 14–19 Ma therefore correspond to the formation of zircon B rims and garnet rims that record the maximum temperature during exhumation. Nevertheless, the large variation (1.8‰ in zircon and 1.6‰ in garnet) of $\delta^{18}O$ values both in garnet and zircon exceed analytical errors (± 0.5–1‰ for zircon, and ± 0.3–0.5‰ for garnet) and reflect intergranular heterogeneity at the rock scale. The absence of complete isotopic equilibrium between minerals at the rock scale might be explained by the impermeable character of the mafic protolith. $\delta^{18}O$ values measured in metamorphic zircon and garnet formed during non-pervasive fluid flow should thus depend on the micro-textural location of the zircon (as inclusions in garnet, at grain boundaries, or in microcracks). Unfortunately, available techniques cannot resolve these issues in this sample. Indeed, the scarcity of zircon practically prevents in situ $\delta^{18}O$ measurements in thin section. Therefore, it is not practical to assess the micro-textural location of

Table 7
Oxygen isotope analyses for zircon from metabasite NA0180b and metasediments NA01113b and NA0262b (additional analyses are given in Tables 4 and 6)

Name of analysis	Domain	$\delta^{18}O$ (‰)	$\pm \sigma$ (‰)
NA0180b			
80b47-c	Core	5.1	0.8
80b47-r1	Rim A	5.1	0.8
*80b3-c	Core	7.3	0.4
*80b3-r1	Rim A	7.1	0.4
*80b16-c	Core	7.1	0.4
*80b16-r1	Rim A	7.4	0.4
*80b16-r2	Rim B	6.7	0.4
80b3-1	Core	5.0	0.9
80b23-2	Rim A	5.5	0.9
*80b17-r2	Rim B	7.6	0.4
*80b17-r2b	Rim B	9.0	0.4
80b38-1	Rim B	8.0	0.9
NA01113b			
113b16-r	Rim	13.7	0.8
113b16-c	Core	4.9	0.8
113b15-r	Rim	12.9	0.8
113b15-c	Core	5.5	0.8
113b26-1	Rim	11.8	0.6
113b26-2	Rim	12.1	0.6
113b26-3	Core	6.6	0.6
NA0262b			
62b20-2	Core	10.7	0.6
62b6-3	Rim	13.6	1.4
62b10	Rim	14.6	1.1
62b10	Core	10.4	1.1
62b9	Core	5.1	1.1
62b12	Rim	14.3	1.1

Note: All samples are prefixed by NA01 (80b, 113b) or NA02 (62b).
*: same sample as NA0180b, but zircon crystals are on a second polished section.
σ on $\delta^{18}O$ value take into account the external and internal errors. The name of isotopic analyses must be read as: name of the sample, name of zircon and name of the analyses.

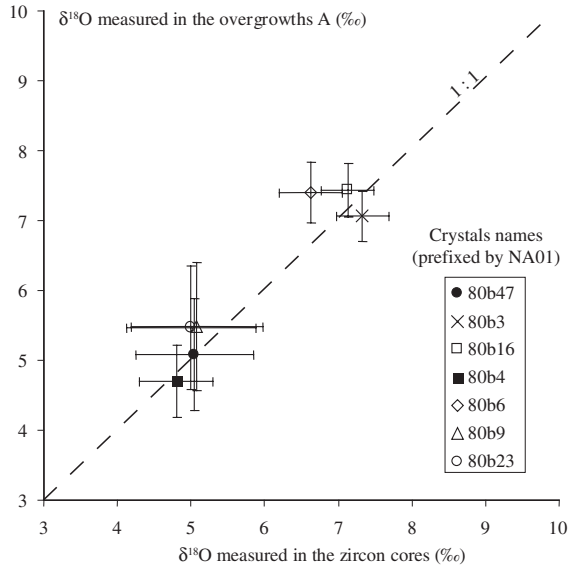

Fig. 10. $\delta^{18}O$ measured in overgrowths A versus $\delta^{18}O$ measured in zircon cores from metabasite NA0180b.

the analysed zircon, and to verify if the hypothesis of local equilibrium among mineral phases is fulfilled.

In metapelite NA0262b, the $\delta^{18}O$ values measured in the zircon metamorphic overgrowths are homogeneous (14.2 ± 0.5‰) and are similar to those measured in the cores of small garnet crystals (14.8 ± 0.2‰). The absence of scatter in $\delta^{18}O$ values measured both in zircon overgrowths and in garnet cores shows that isotopic equilibrium was readily achieved during their formation at the rock scale. As zircon overgrowths have been dated at ca. 50 Ma by U–Pb isotopes, it seems that garnet cores and zircon overgrowths both preserve a record of M1 metamorphism. Moreover, using the partition coefficient from Zheng (1993), the calculated $\delta^{18}O$ value for fluid in equilibrium with both minerals is ca.17‰ for a temperature range of 400–670 °C, which is consistent with $\delta^{18}O$ values of Naxos prograde fluids ($12‰ < \delta^{18}O < 16‰$, Baker et al., 1989).

In calcic gneiss NA01113b, zircon overgrowths have a $\delta^{18}O$ value of 11.8 ± 1.4‰. This value is similar to the $\delta^{18}O$ measured in garnet rims (11.4 ± 1.1‰). The U–Pb ages obtained in zircon overgrowths (ca. 50 Ma), the similarity between $\delta^{18}O$ values measured in garnet rims and zircon overgrowths, and the signature of fluids in equilibrium with garnet rims (14‰) are all consistent with concomitant growth of garnet rims and zircon overgrowths during M1.

The three samples studied correspond to three lithologies, with different permeabilities, that underwent heating up to 660 °C (Wijbrans, 1985; Jansen and Schuiling, 1976). But in each case, the zircon rim and garnet growth zones can be associated thanks to their $\delta^{18}O$ values. Moreover, in each case, the U–Pb ages in zircon rims and the $\delta^{18}O$ value preserved in garnet and zircon correspond to the characteristics of one of the two metamorphic events previously identified at Naxos. Moreover, in samples NA0262b and NA01113b, the $\delta^{18}O$ values corresponding to the M1 event are preserved despite the superimposed M2 high-temperature event. Even though experimental data predict oxygen diffusion over 25 μm at 600–650 °C after 5 Ma in hydrous conditions (Zheng and Fu, 1998; Cherniak and Watson, 2003), the above observations do not provide evidence of any perturbation through post-growth diffusion. Oxygen isotopes appear to be a powerful tool to relate garnet and zircon growth even under high grade metamorphism and in the presence of fluid.

7. Conclusion

Metamorphic zircon overgrowths have been identified in metamorphic rocks occurring around the migmatitic core in Naxos. They have characteristic morphologies (either by the absence of zoning or by chaotic zoning), and their chemical composition (rich in HfO_2 and poor in trace elements with respect to magmatic zircon). Zircon metamorphic crystallisation is correlated with garnet growth and fluid circulation using oxygen isotope geochemistry. This method is a powerful tool for deciphering the mechanism of growth, and for constraining zircon crystallisation in the metamorphism history. However, this method is potentially hampered by (1) the inability to verify the textural equilibrium state of zircon with the other mineral phases and (2) the possible preservation in metamorphic overgrowths of ancient isotopic signatures from pre-existing zircon when they form by in situ recrystallisation. The preservation of pre-existent $\delta^{18}O$ signatures in zircon is related to the nature of the fluid/rock interaction that occurs during metamorphism. Metamorphic zircon from metabasites, broadly

resistant to fluid infiltration, retains the isotopic signature of the pre-existent magmatic zircon. In contrast, metamorphic zircon from metapelite, in which fluids are pervasive, is in isotopic equilibrium with those fluids. These cases exemplify two end-members of recrystallisation processes, in the solid-state or dissolution–reprecipitation.

Three stages of metamorphic zircon growth were dated at 55, 45, and 16 Ma. Nevertheless, the two first events correspond to similar pressure–temperature conditions (a high pressure low temperature environment, corresponding to prograde garnet growth) and stable isotope fluid composition ($\delta^{18}O$ values for fluids in equilibrium with zircon higher than 12‰). These conditions prevailed during a period of ca. 10 Ma. The last event took place in a medium pressure (MP)–medium temperature (MT) environment, characterised by circulation of low $\delta^{18}O$ (<10‰) fluids.

Although the MP–MT M2 metamorphism event is apparently dominant in the field and petrographically, garnet and zircon have largely preserved a record of the earlier high pressure–low temperature M1 metamorphic event.

Acknowledgements

This work was funded by CNRS IT-programs 2001, 2002, and UHP BQR 2000.

We thank F. Diot, A. Kohler, and J. Ravaux for their assistance for SEM and cathodoluminescence imaging, and electron microprobe analyses. We are also grateful to D. Mangin and M. Champenois for their help with SIMS measurements. The quality of the manuscript was improved by careful reviews by P. Hoskin, M. Whitehouse and B. Bingen.

References

Andriessen, P.A.M., 1991. K–Ar and Rb–Sr age determinations on micas of impure marbles of Naxos, Greece: the influence of metamorphic fluids and lithology on the blocking temperature. Schweizerische Mineralogie und Petrologie Mitteilungen 71, 89–99.

Andriessen, P.A.M., Boelrijk, N.A.I.M., Hebeda, E.H., Priem, H.N.A., Verdurmen, E.A.T., Verchure, R.H., 1979. Dating the events of metamorphism and granitic magmatism in the Alpine Orogen of Naxos (Cyclades, Greece). Contributions to Mineralogy and Petrology 69, 215–225.

Avigad, D., 1998. High-pressure metamorphism and cooling on SE Naxos (Cyclades, Greece). European Journal of Mineralogy 10, 1309–1319.

Baker, J., Bickle, M.J., Buick, I.S., Holland, T.J.B., Matthews, A., 1989. Isotopic and petrological evidence for the infiltration of water-rich fluids during the Miocene M2 metamorphism on Naxos, Greece. Geochimica et Cosmochimica Acta 53, 2037–2050.

Bingen, B., Austrheim, H., Whitehouse, M.J., 2001. Ilmenite as a source for zirconium during high-grade metamorphism? Textural evidence from the Caledonides of western Norway and implications for zircon geochronology. Journal of Petrology 42, 355–375.

Chakraborty, S., Ganguly, J., 1992. Cation diffusion in aluminosilicate garnets: experimental determination in spessartine–almandine couples, evaluation of effective binary diffusion coefficients, and applications. Contributions to Mineralogy and Petrology 111, 74–96.

Cherniak, D.J., Watson, E.B., 2000. Pb diffusion in zircon. Chemical Geology 172, 5–24.

Cherniak, D.J., Watson, E.B., 2003. Diffusion in zircon. Reviews in Mineralogy and Geochemistry, 113–143.

Corfu, F., Hanchar, J.M., Hoskin, P.W.O., Kinny, P.D., 2003. Atlas of zircon textures. Reviews in Mineralogy and Geochemistry 53, 469–500.

Cygan, R.T., Lasaga, A.C., 1985. Self diffusion of magnesium in garnet at 750 to 900 °C. American Journal of Science 285, 328–350.

Deloule, E., Alexandrov, P., Cheilletz, A., Laumonier, B., Barbey, P., 2002. In situ U–Pb zircon ages for Early Ordovician magmatism in the eastern Pyrenees, France: the Canigou orthogneisses. International Journal of Earth Science (Geologisches Rundschau) 91, 398–405.

Eiler, J.M., Graham, C.M., Valley, J.W., 1997. SIMS analysis of oxygen isotopes: matrix effects in complex minerals and glasses. Chemical Geology 138, 221–244.

Eiler, J.M., Schiano, P., Kitchen, N., Stolper, E.M., 2000. Oxygen-isotope evidence for recycled crust in the sources of mid-ocean-ridge basalts. Nature (London) 403, 530–534.

Elphick, S.C., Ganguly, J., Loomis, T.P., 1985. Experimental determination of cation diffusivities in aluminosilicate garnets. Contribution to Mineralogy and Petrology 90, 36–44.

France-Lanord, C., Sheppard, S.M.F, LeFort, P., 1988. Hydrogen and oxygen variations in the high Himalaya peraluminous Manaslu leucogranite; evidence for heterogeneous sedimentary source. Geochimica et Cosmochimica Acta 52, 513–526.

Fraser, G., Ellis, D., Eggins, S., 1997. Zirconium abundance in granulite-facies minerals, with implications for zircon geochronology in high-grade rocks. Geology 25, 607–610.

Gebauer, D., Schertl, H.P., Brix, M., Schreyer, W., 1997. 35 Ma old ultrahigh-pressure metamorphism and evidence for very rapid exhumation in the Dora Maira Massif, western Alps. Lithos 41, 5–24.

Hermann, J., Rubatto, D., Korsakov, A., Shatsky, V.S., 2001. Multiple zircon growth during fast exhumation of diamondiferous,

deeply subducted continental crust (Kokchetav Massif, Kazakhstan). Contributions to Mineralogy and Petrology 141, 66–82.
Hoskin, P.W.O., Black, L.P., 2000. Metamorphic zircon formation by solid-state recrystallisation of protolith igneous zircon. Journal of Metamorphic Geology 18, 423–439.
Hoskin, P.W.O., Ireland, T.R., 2000. Rare earth element chemistry of zircon and its use as a provenance indicator. Geology 28, 627–630.
Hoskin, P.W.O., Schaltegger, U., 2003. The composition of zircon and igneous and metamorphic petrogenesis. Reviews in Mineralogy and Geochemistry 53, 27–62.
Ireland, T.R., 1995. Ion microprobe mass spectrometry: techniques and applications in cosmochemistry, geochemistry, and geochronology. Advances in Analytical Geochemistry 2, 1–118.
Jansen, J.B.H., 1973. Geological Map of Greece, Island of Naxos. Institute for Geology and Mineral Resources, Athens. 341 pp.
Jansen, J.B.H., Schuiling, R.D., 1976. Metamorphism on Naxos: petrology and geothermal gradients. American Journal of Science 276, 1225–1253.
Keay, S., 1998. The geological evolution of the Cyclades, Greece. Constraints from SHRIMP U–Pb geochronology. PhD Thesis, Australian National University, Canberra. 335 pp.
Keay, S., Lister, G., Buick, I., 2001. The timing of partial melting, Barrovian metamorphism and granite intrusion in the Naxos metamorphic core complex, Cyclades, Aegean Sea, Greece. Tectonophysics 342, 275–312.
Lee, J.K.W., Williams, I.S., Ellis, D.J., 1997. Pb, U and Th diffusion in natural zircon. Nature 390, 159–161.
Möller, A., O'Brien, P.J., Kennedy, A., Kröner, A., 2002. Polyphase zircon in ultrahigh-temperature granulites (Rogaland, SW Norway): constraints for Pb diffusion in zircon. Journal of Metamorphic Geology 20, 727–740.
Pan, Y., 1997. Zircon- and monazite-forming metamorphic reactions at Manitouwadge, Ontario. The Canadian Mineralogist 35, 105–118.
Peucat, J.-J., Hirata, T., Nesbitt, R.W., 1995. REE fractionation (ICPMS LASER) evidence in metamorphic zircon during granulite facies metamorphism and anatectic processes. Terra Abstracts 7, 346.
Pidgeon, R.T., 1992. Recrystallisation of oscillatory zoned zircon: some geochronological and petrological implications. Contributions to Mineralogy and Petrology 110, 463–472.
Pidgeon, R.T., Nemchin, A.A., Hitchen, G.J., 1998. Internal structures of zircons from Archaean granites from the Darling Range Batholith; implications for zircon stability and the interpretation of zircon U–Pb ages. Contributions to Mineralogy and Petrology 132, 300–306.
Rizvanova, N.G., Levchenkov, O.A., Belous, A.E., B., N.I., Maslenikov, A.N., Komarov, A.N., Makeev, A.F., Levskiy, L.K., 2000. Zircon reaction and stability of the U–Pb isotope system during interaction with carbonate fluid: experimental hydrothermal study. Contributions to Mineralogy and Petrology 139, 101–114.
Roberts, M.P., Finger, F., 1997. Do U–Pb zircon ages from granulites reflect peak metamorphic conditions? Geology 25, 319–322.
Rubatto, D., 2002. Zircon trace element geochemistry: partitioning with garnet and the link between U–Pb ages and metamorphism. Chemical Geology 184, 123–138.
Schaltegger, U., Fanning, M., Günther, D., Morin, J.C., Schulmann, K., Gebauer, D., 1999. Growth annealing and recrystallisation of zircon and preservation of monazite in high grade metamorphism: conventional and in situ U–Pb isotope, cathodoluminescence and microchemical evidence. Contributions to Mineralogy and Petrology 134, 186–201.
Spear, F.S., 1993. Metamorphic Phase Equilibria and Pressure–temperature–time Paths. Mineralogical Society of America Monograph. 799 pp.
Stacey, J.C., Kramers, J.D., 1975. Approximation of terrestrial lead isotopes evolution by a two stage model. Earth and Planetary Science Letters 26, 207–221.
Valley, J.W., Chiarenzelli, J.R., McLelland, J.M., 1994. Oxygen isotope geochemistry of zircon. Earth and Planetary Science Letters 126, 187–206.
Valley, J.W., Kitche, N., Kohn, M.J., Niendorf, C.R., Spicuzza, M.J., 1995. UWG-2, a garnet standard for oxygen isotope ratios; strategies for high precision and accuracy with laser heating. Geochimica et Cosmochimica Acta 59, 5223–5231.
Vanderhaeghe, O., 2004. Structural record of the Naxos dome formation. In: Whitney, D.L., Teyssier, C., Siddoway, C.S. (Eds.), Gneiss Domes in Orogeny, Geological Society of America Special Paper.
Vielzeuf, D., Champenois, M., Valley, J.W., Brunet, F., 2003. SIMS analyses of oxygen isotopes: matrix effects in Fe–Mg–Ca garnets. Geophysical Research Abstracts 5, 10926.
Whitehouse, M.J., Platt, J.P., 2003. Dating high-grade metamorphism-constraints from rare-earth elements in zircon and garnet. Contributions to Mineralogy and Petrology 145, 61–74.
Wiedenbeck, M., Alle, P., Corfu, F., Griffin, W.L., Meier, M., Oberli, F., Von Quadt, A., Roddick, J.C., Spiegel, W., 1995. Three natural zircon standards for U–Th–Pb, Lu–Hf, trace element and REE analyses. Geostandards Newsletter 19, 1–23.
Wijbrans, J.R., 1985. Metamorphic histories by the $^{40}Ar/^{39}Ar$ age spectrum method. PhD Thesis, A.N.U., Canberra.
Wijbrans, J.R., McDougall, I., 1986. $^{40}Ar/^{39}Ar$ dating of white micas from an Alpine high-pressure metamorphic belt on Naxos (Greece): the resetting of the argon isotopic system. Contributions to Mineralogy and Petrology 93, 187–194.
Williams, I.S., Buick, I.S., Cartwright, I., 1996. An extended episode of Early Mesoproterozoic fluid flow in the Reynolds Range, central Australia. Journal of Metamorphic Geology 14, 29–47.
Zeck, H.P., Whitehouse, M.J., 1999. Hercynian Panafrican Proterozoic and Archean ion microprobe zircon ages for a Betic-Rif core complex, Alpine belt, W. Mediterranean. Consequences for its *P–T–t* path. Contributions to Mineralogy and Petrology 134, 134–149.
Zheng, Y.F., 1993. Calculation of oxygen isotope fractionation in anhydrous silicate minerals. Geochemica et Cosmochimica Acta 57, 1079–1091.
Zheng, Y.F., Fu, B., 1998. Estimation of oxygen diffusivity from anion porosity in minerals. Geochemical Journal 32, 71–89.